Shock induced fluid structure interaction on a flexible wall in supersonic turbulent flow

Sebastian Willems⋆, Ali Gülhan⋆ and Burkard Esser⋆
⋆German Aerospace Center (DLR), Institute of Aerodynamics and Flow Technology,
Supersonic and Hypersonic Technology Department, Linder Höhe, 51147 Köln, Germany

Abstract

A detailed knowledge of the flow structure interaction in supersonic flows is important for the design of future space transportation systems. Therefore this work was devoted to the investigation of the shock wave boundary layer interaction on an elastic panel. During the wind tunnel experiments the panel deflection was measured with fast non-intrusive displacement sensors. On the flow side pressure, high-speed Schlieren photography and oil-film technique were used. The flow manipulation due to the panel deflection becomes manifest in a deformation of the impinging shock and the separation zone. The panel deflection consists of a constant and a dynamic component. The experimental results are discussed and compared to numerical results.

1. Introduction

The propulsion unit is one of the driving parameters of the costs and reliability of future space transportation systems. A design approach approach based on experiments is not feasible because of the high costs of construction, manufacturing and testing. Therefore the development of reliable numerical tools is important for design and optimization. But such tools have to include several complex flow and structure properties such as; real gas effects, multiphase flow, base flow, regenerative and film cooling, structure deformation and degeneration, anisotropic materials, flow separation and shock wave boundary layer interaction. The objective of the collaborative research program "Transregio 40" is to combine and improve the tools and approaches of the different disciplines for a proper integrated interdisciplinary design process. Beside the numerical projects the program includes also several experimental projects for the verification of developed physical models and numerical tools. This requires deepening of the comprehension of key mechanisms and the invention of new models. A key factor for the nozzle design is the comprehension of the fluid structure interactions in supersonic flows [12] [10]. Therefore it was the topic of several numerical [14] [19] and experimental investigations [16] [20].

The wind tunnel experiments performed at the Supersonic and Hypersonic Technology Department of the German Aerospace Center in Cologne with a generic model and well defined boundary conditions allow the comparison with high order numerical simulations. The experimental set-up includes the fundamental and well reviewed problem of a shock wave impingement on the turbulent boundary layer of a flat plate [3] [4] [11] and extends it by using an elastic panel allowing a two-dimensional deformation. It combines the aspects of compressibility, flow separation, turbulence and aeroelasticity. In order to detect the influence of the interaction and to facilitate the validation of the numerical tools the structure deformation and the shock wave boundary layer interaction were also examined separately.

During the experiments the flow parameters were measured with standard techniques such as pressure sensors, high-speed Schlieren photography and oil-film technique. The panel deflection was measured via non-intrusive displacement sensors. For a detailed knowledge of the inflow parameter the turbulent intensity and the boundary layer profile were measured with a Laser-2-Focus Velocimeter and a miniature Pitot rake, respectively.

This paper presents the main results of the experiments combining a shock wave boundary layer interaction (SWBLI) with a fluid structure interaction (FSI) and comparing them with some numerical simulations.
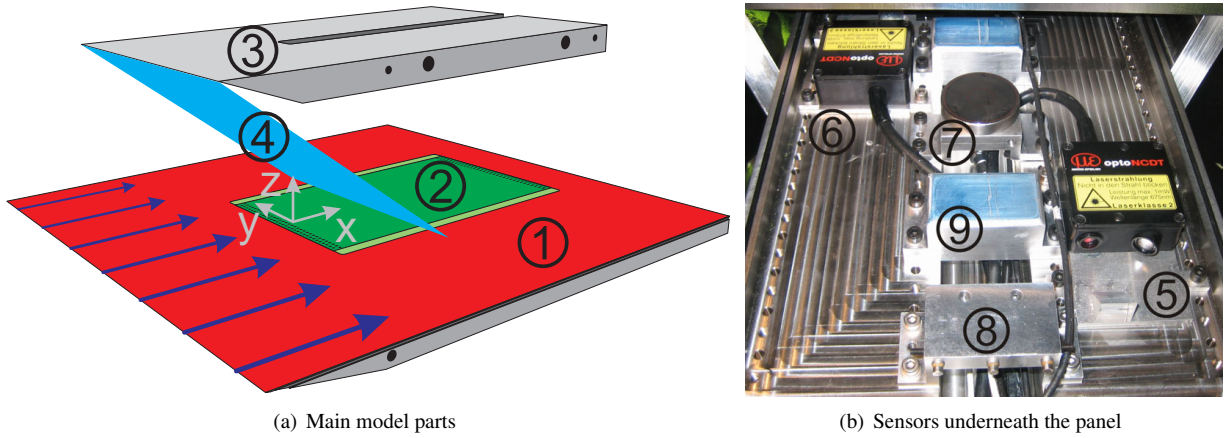
(a) Main model parts

(b) Sensors underneath the panel

Figure 1: Experimental set-up and instrumentation

2. Experiment set-up

2.1 The model

The generic model used for the experiments was designed for the research into fluid structure interactions and the verification of coupled flow-structure simulations. The requirements include well defined boundary conditions, a non-intrusive but fast measurement of the flow and the structural characteristics, a flexible set-up for sensitivity analysis and the possibility to break a complex flow-structure interaction down to the basic effects. In addition it should be (distantly) related to the situation of an over-expanded nozzle flow with a cap-shock and thereby induced separation on the nozzle wall [15].

The experiment set-up is shown in figure 1(a). It consists of a quadratic base plate ① that spans the whole wind tunnel width. It has a sharp leading edge with a 10° ramp angle to the bottom side. A 5 mm wide stripe of F150-macrogrits ($\approx 60 \, \mu$m grains) behind the leading edge trips the boundary layer (see also Section 3.1). A frame is inserted into the base plate, which carries an elastic sheet metal ② made of 1.47 mm thick spring steel (CK 75). Two rows of rivets at the front side as well as at the rear side of the panel realize restrictive grips. The other two sides of the panel are not restricted but a thick layer of a soft type foam rubber between the underside of the elastic panel and a frame's ledge seals the chamber underneath the elastic panel towards the flow. The pressure equalization of this chamber was initially done at a point downstream of the plate where the pressure is similar to the static pressure of the inflow and later at a feedthrough in the wind tunnel wall upstream the model. Above the plate there is a 20° wedge ③, which generates a shock ④ that hits the elastic panel. The wedge is 300 mm wide and its position can be varied in flow direction. For the examination of the shock wave boundary layer interaction without a structural deflection a rigid insert can be mounted into the base plate. The origin of the coordinate system used in this paper is the midpoint of the leading grip's edge. The X-axis is defined in flow direction and the Z-axis is defined orthogonal to the baseplate upwards (see figure 1(a)).

2.2 Test facility

The experiments were carried out in the Trisonic Test Section (TMK) in Cologne. It is a blowdown wind tunnel with a closed test section of $0.6 \, \text{m} \times 0.6 \, \text{m}$. A continuously adjustable nozzle enables the complete Mach number range from 0.5 to 5.7. An ejector allows experiments with reduced static pressure. Thus the unit Reynolds number can be varied between $7 \cdot 10^6 \, \frac{1}{\text{m}}$ and $43 \cdot 10^6 \, \frac{1}{\text{m}}$ at Mach 3.0. The maximum test time is about 60 seconds. (For further details see [5].) The typical test conditions for the Mach numbers used in the experiments are listed in tabular 2.2.

2.3 Data acquisition

The flow parameters of the inflow are recorded by temperature and pressure sensors in the settling chamber of the wind tunnel. Schlieren pictures taken by a Photron FASTCAM APX RS high-speed camera allow a time accurate detection

Table 1: Flow parameters of the experiments

Ma [ ]	Ejector	p_∞ [kPa]	T_∞ [K]	$v_\infty \left[\frac{m}{s}\right]$	$Re \left[\frac{10^6}{m}\right]$
2.5	-	21.5	128.9	569	37.0
3.0	-	15.9	103.6	612	45.6
3.5	-	12.0	84.1	643	55.4
4.0	-	9.1	69.0	666	65.2
4.5	-	7.1	57.4	684	77.6
3.0	1.2 MPa	8.3	103.6	612	23.8

of the shock positions. For most experiments the image section was 1024×512 pixels and the sampling rate 5 kHz, for some experiments the section was reduced to 512×256 pixels to increase the sampling rate to 20 kHz. The image analysis was done with the help of the OpenCV library [1] using a Gaussian filter and the Canny edge detection algorithm and is thereby similar to the one described by Estruch et al. [6]. In addition, a software image stabilization algorithm was utilized.

Three pressure sensors (Kulite XTL-DC-123C-190) are placed upstream, downstream and inside the sealed chamber. Underneath the elastic panel there are several displacement sensors (Fig. 1(b)) to measure the deflection of the elastic panel. Two laser triangulation sensors optoNCDT 1607-10 from Micro-Epsilon ⑤&⑥ allow point measurements with 10 kHz. A capacitive displacement sensor capaNCDT 6350-5 from Micro-Epsilon ⑦ enables more precise measurements at sample rates up to 50 kHz. Three capacitive displacement sensors HPC-75 from Capacitec ⑧ measure the deflection of the frame at one grip. There are also two pads ⑨ limiting the maximum deflection to 4.5 mm and thus avoiding the elastic panel hitting the sensors. To gain more information about the deflection shape, the displacement sensors can be placed at several positions under the panel.

The static results of the sensors were processed by averaging all data points of 10 seconds steady state flow. For the frequency spectra of the sensor measurements and the shock positions the gained data are divided into several blocks with an overlap of 50 %. After multiplying with the Hann function the power spectral density is processed for each block and then the arithmetic average of all block results is computed.

The oil-film technique [13] was used to determine the shape of the shock boundary layer interaction zone and the size of the recirculation region on the rigid and the elastic panel. For the pure deflection experiments the elastic panel was equipped with pairs of strain gauges in half bridge configuration. The rigid insert is equipped with two rows of static pressure probes (PSI) every 10 mm. One row is on the symmetry axis and the other one in 90 mm distance.

3. Preliminary experiments

The preliminary experiments were performed to determine the exact boundary conditions of the test facility and the model. This is important for the comparison with high quality simulations.

3.1 Flow characterisation

The turbulent intensity and velocity in the undisturbed inflow were directly measured with a Laser-2-Focus Velocimeter. It measures the point velocity distribution of particles in the flow in a single direction with the help of two focused laser beams as shown in figure 2(a) (for further details see [18]). Therefore the flow was seeded with an oil aerosol at the end of the settling chamber. The turbulent intensity was thereby quantified to a value of 2.0 % in streamwise direction and 2.5 % in orthogonal direction. This matches the estimation for a fully developed pipe flow [7] of 1.9 % for $Re_{D_H} = 30 \cdot 10^6$.

$$I = \frac{0.16}{\sqrt[8]{Re_{D_H}}} \tag{1}$$

The measured velocities were about 1.5 % lower than the values calculated with the help of the isentropic equations for a de Laval nozzle.

For the numerical simulations it was also important to guarantee a fully developed turbulent boundary layer and to characterize the boundary layer in detail. Therefore a miniature Pitot rake was mounted onto a plate with the same shape as the base plate 150 mm from the tip (which equates 70 mm upstream the elastic panel). It has ten tubes with

(a) Concept draft of the Laser-2-Focus Velocimeter
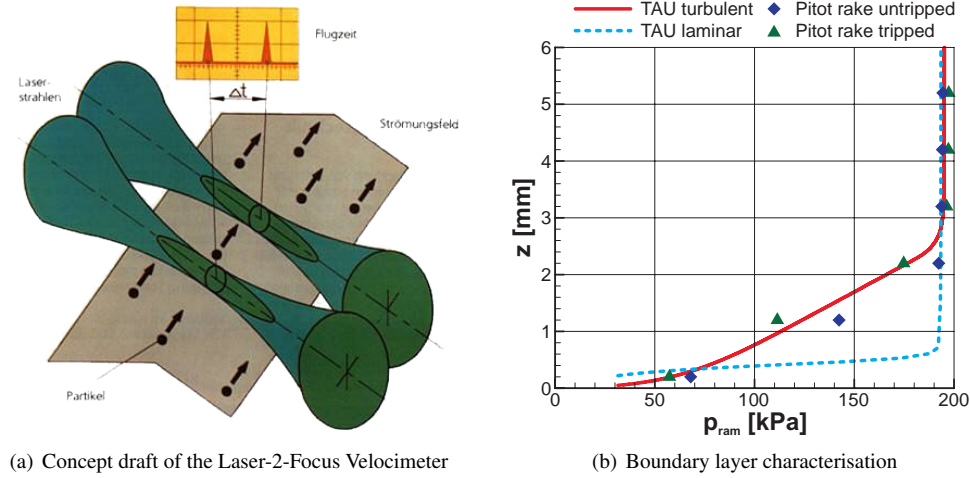
(b) Boundary layer characterisation

Figure 2: Experiments for flow characterisation

an inner diameter of 0.2 mm and an outer diameter of 0.4 mm. The measured ram pressures with and without tripping at the leading edge were compared to the results of a fully turbulent and a laminar simulation with the numerical flow solver TAU using a Wilcox-k-ω turbulence model (Fig. 2(b)).

3.2 Structural behavior under a static uniform load

To determine the pure deflection characteristic of the elastic panel additional experiments with a static uniform pressure load were performed. Therefore the pressure underneath the elastic panel was reduced. The maximum deflection against the pressure difference is plotted in figure 3(a), for the discussion of the additional numerical results see chapter 4.1. Figure 3(b) shows the measured deflection of the frame were the elastic panel is fixed. Obviously the grip is not ideally restrained, but there is a repeatable measurable deflection.

To gain more information about the deflection, the tensile strain in the elastic panel was measured at several positions with the help of strain gauges. The measured tensile strain against the deflection is plotted in figure 3(e). The positions and the orientation of the strain gauge pairs are shown above figure 3(f). The sensors ■, ◆ and ▲ are placed on the longitudinal symmetry plane and measure in the longitudinal direction. While ■ is placed right in the middle of the panel, ▲ is placed close to the grip and ◆ in the middle between those two. As expected all three measure similar tensile strains, but much less than the strain which can be derived from the curve elongation. By adjusting the tensile force N in the beam equation 2, so that it matches the measured maximum deflections, we get a 'corrected' beam equation, which computes similar strains. The strain gauge pair ● is placed close to a free side of the panel and also measures in longitudinal direction. There the tensile strains are significantly lower than in the symmetry plane, also ▼ is placed between ■ and ● and measures a compression in transverse direction.

4. Numerical simulations

The numerical results presented in this paper are not based on the tools developed within the Transregio 40 and carried out with more simple models and existing tools. The aim was not to perform high quality simulations including all involved effects but to evaluate and explain the experimental results. In addition, the comparison indicates the requirements for numerical simulations and the options of verification. (For detailed information concerning the numerical simulations developed within the Transregio 40 and connected to the presented experiments please refer to Schieffer et al. [17], Grilli et al. [9] and Danowski and Wall [2].)

4.1 Numerical simulation of the structure deflection

A first approximation of the structural deflection under a static uniform pressure load gives the second order beam equation (2). In contrast to the linear first order beam equation it considers the tensile force N derived from the
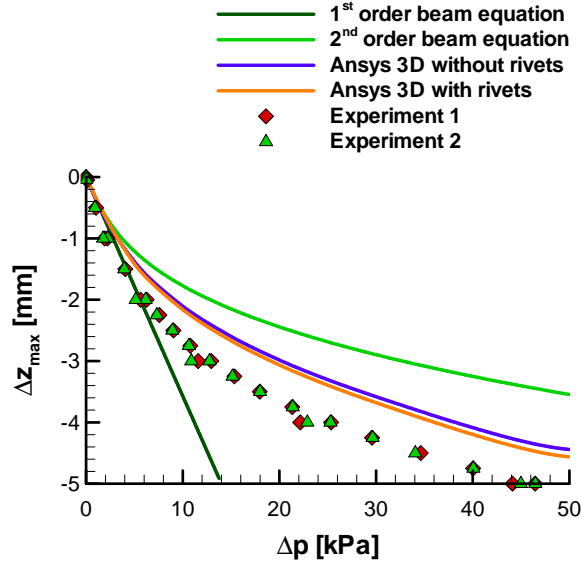
(a) Deflection of the panel vs. pressure difference
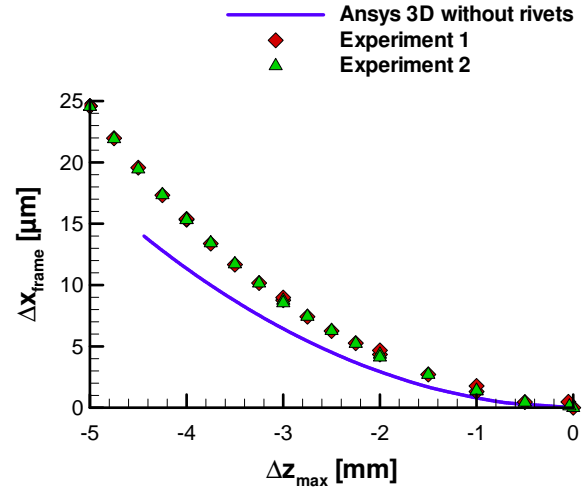
(b) Deflection of the grip vs. deflection of the panel
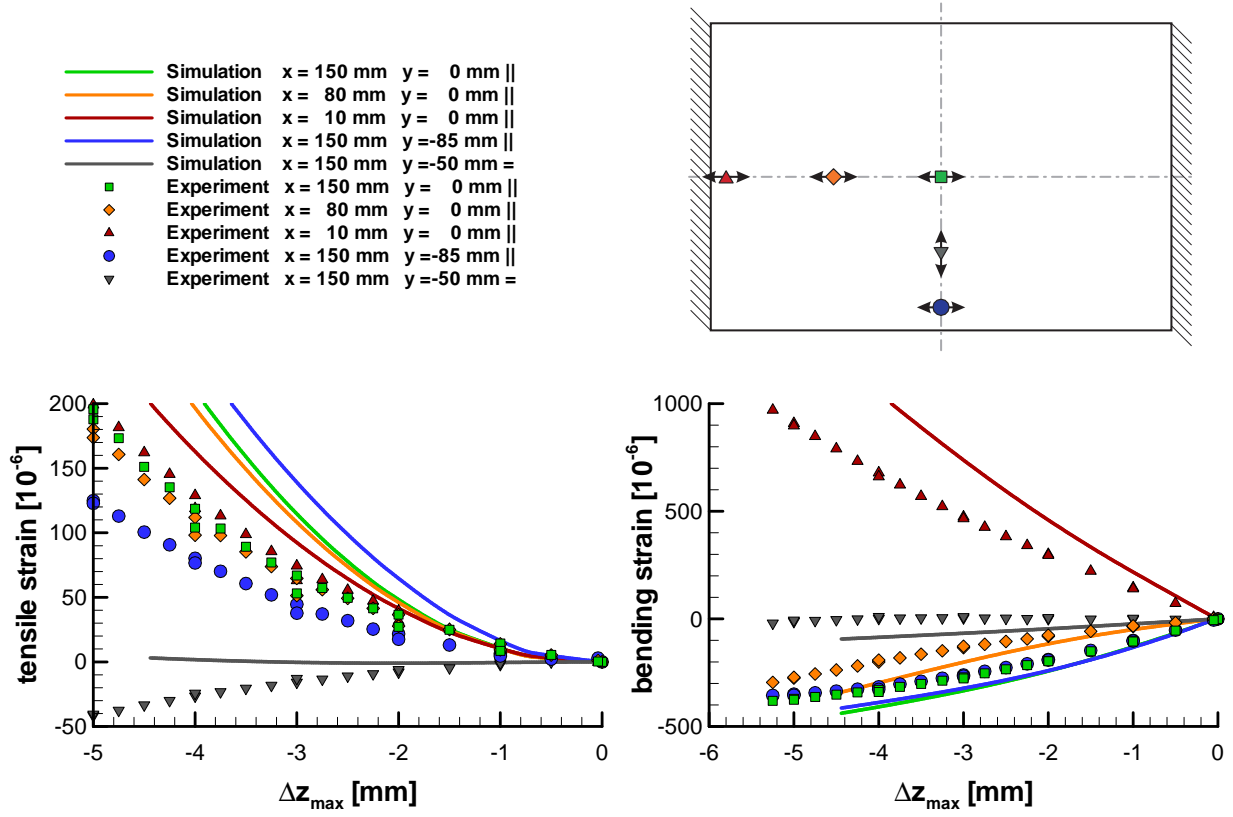
(e) Tensile strains of the panel vs. deflection of the panel

(f) Bending strains of the panel vs. deflection of the panel

Figure 3: Deflection of the elastic panel due to a static uniform load

(a) Static deflection (with rivets)

(b) Normal mode 1; 2 (without rivets)

Figure 4: 3D finite element simulation for a static uniform pressure load of 30 kPa

geometric curve elongation ε and the Young's modulus E. The calculations match the results of a 2D finite element simulation using Ansys and the option "large deflections".

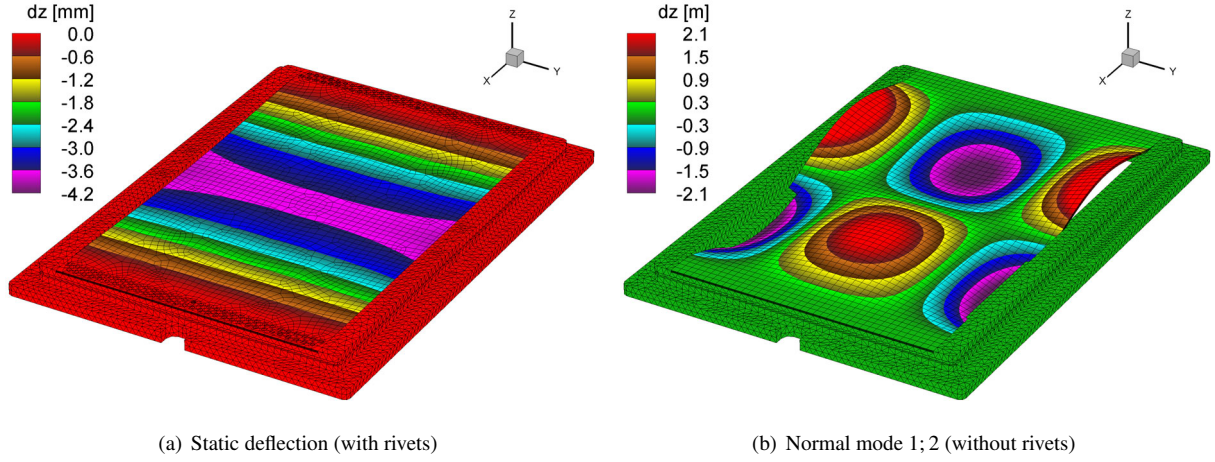$$w''''(x) = \frac{q(x) + Nw''(x)}{E \cdot I} \qquad \wedge \qquad N = EA\varepsilon = \frac{EA}{l}\left[\int_0^l \sqrt{1 + [w'(x)]^2}\, \mathrm{d}x - l\right] \qquad (2)$$

But the results of a 3D simulation including the frame of the elastic panel are much closer to the measured deflections (Fig. 3(a)). In addition it shows, that the deflection of the panel at the borders is greater than in the middle. This is shown in figure 4(a) for a static uniform pressure load of 30 kPa. A further but small improvement of the model can be achieved by replacing the fixed connection between the panel and frame with a (ideal) model of the rivets. For fast valuable estimations of the panel deflection the second order beam equation can be fitted to the experimental results by multiplying the tensile force with $\left(e^{-7500\varepsilon} + 0.5\right)$.

The full 3D finite element model allows an estimation of the normal modes of the elastic panel for various deflections. As it is common usage the modes are named by the number of neutral lines in longitudinal (X-direction) and transverse (Y-direction) direction. Hence figure 4(b) shows the normal mode 1; 2 for the static pressure load of 30 kPa. The first normal modes for several deflections are given in table 4.1. As expected the frequencies of the normal modes increase with the deflection. But the amount of the frequency increase depends on the mode. In general, the relative frequency increase is bigger for lower modes. Therefore the order of the normal modes regarding their frequency is not constant. For example in the case of no or just slight deflection ($\Delta p \leq 2\,\text{kPa}$) the frequency of the mode 0; 2 is lower than mode 1; 1 and the frequency of the mode 3; 0 is lower than mode 1; 3 but for bigger deflections ($\Delta p \geq 10\,\text{kPa}$) it is just the other way round.

Table 2: Frequencies of the first normal modes of the elastic panel with an uniform pressure load

Δp [kPa]	$\Delta z_{\max}$ [mm]	Normal modes [Hz] 0; 0	0; 1	1; 0	0; 2	1; 1	1; 2	2; 0	2; 1	0; 3	2; 2	3; 0	1; 3	3; 1	3; 2
0	0.0	88	123	242	284	294	471	475	534	626	730	785	807	850	1058
2	−0.7	96	130	246	291	298	474	482	541	629	734	789	809	856	1063
10	−2.1	154	187	282	342	332	499	528	587	659	770	834	828	905	1104
20	−3.0	197	231	317	388	365	528	571	631	688	804	880	850	953	1144
30	−3.6	226	263	345	422	392	552	604	663	711	831	918	868	992	1177

4.2 Numerical simulation of the flow field

To test the feasibility of the experiments for code verifications and for preliminary comparisons 2D and 3D simulations with an even and an a priori deflected panel were performed using the numerical flow solver TAU [8]. On the one

(a) 3D simulation of stream traces and pressure distribution on an undeflected (left) and an a priori deflected panel (right)

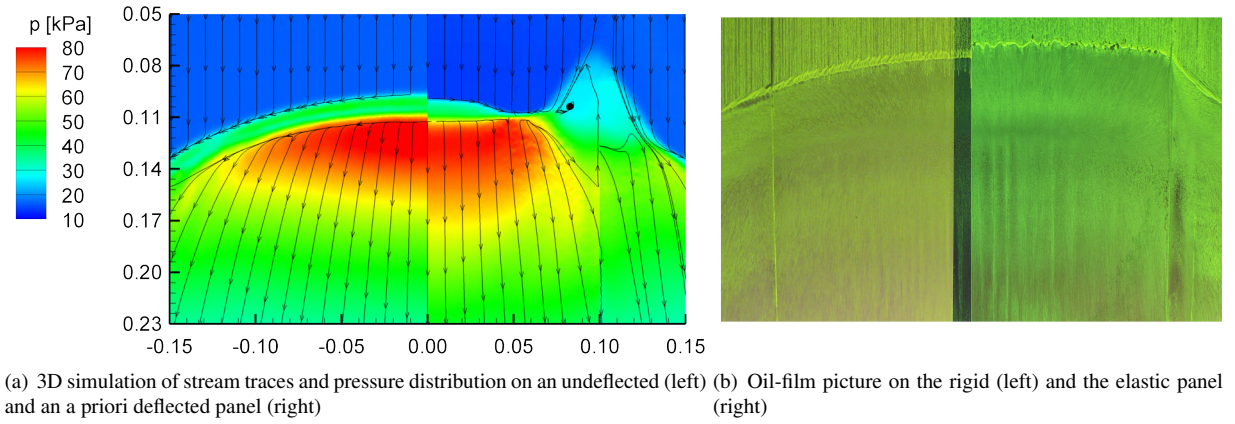(b) Oil-film picture on the rigid (left) and the elastic panel (right)

Figure 5: Shock shape and separation region at Mach 3.0 on an undeflected and a deflected panel

hand they show the high dependency of the prediction of the separation bubble at the shock impingement to the used turbulence model. On the other hand the results show that 2D simulations are good for first approximations but high quality simulations have to be 3D.

Figure 7(a) shows several pressure distributions of the shock wave boundary layer interaction processed by 2D RANS simulations with different turbulence models. All of them predict a major pressure jump at $x = 100$ mm caused by the impinging shock wave and a smaller pressure increase in front caused by the separation bubble respectively the separation shock. The size of the predicted separation and the hight of the pressure jump depend on the used turbulence model. As the ramp of the wedge is just 30 mm high and followed by a plane parallel to the base plate the shock wave is followed by expansion waves. This leads to a pressure decrease after the pressure jump which is same for all turbulence models.

The two major 3D effects of the shock wave boundary layer interaction are caused by the wedge not spanning the whole wind tunnel width. The first effect is a bending of the wedge's shock wave in the Y-direction as it is shown in figure 5(a). The second effect is the greater expansion and therefore steeper decrease of the pressure behind the shock wave due to a flow around the sides of the wedge. This reveals the comparison of the pressure distributions comming from 2D and 3D simulations in figure 7(a) (the higher pressure jump of the 3D simulations is probably caused by a lower grid resolution).

The 2D and 3D simulations with an a priori deflected panel already predict the dominant effects confirmed by the experiments later on. Figure 10 shows the shape of the separation for a (maximum) deflection of 5 mm, 3 mm and the undeflected case using a Wilcox-k-ω turbulence model. Obviously the separation bubble grows in longitudinal as well as transversal direction. In the background the Mach number distribution of the undeflected case is plotted.

Although the grid resolution of the 3D simulation with a deflected panel is insufficient in the region the step between panel and the base plate a straightening of the impinging shock wave can be observed and the formation of a corner vortex at the edge interface of panel and plate suspected.

5. Experimental results

5.1 Shock wave boundary layer interaction on a rigid panel

The main aim of the experiments with a rigid panel was to get a reference state for each Mach number to detect the differences caused by the fluid structure interaction. In addition any malfunction or interference of the distance sensors due to the vibrations and annoyance of a wind tunnel run could have been identified.

Figure 6(a) shows a Schlieren photograph of the shock wave boundary layer interaction at Mach 3.0. Good to see are the shock wave from the wedge ① but also some perturbations from the plate's leading edge ②, the tripping ③ and the rivets ④. At the impingement point a separation bubble forms ⑥ and the shock is reflected ⑤. Obviously the boundary layer is much thicker after the interaction region ⑦. Although there is a considerable fluctuation of the separation bubble in the high-speed Schlieren photographs, there is no prominent frequency in the spectrum analysis of the reflected shock position comparable to the ones described by Dupont et al. [4] and Estruch et al. [6] as shown in figure 6(b).
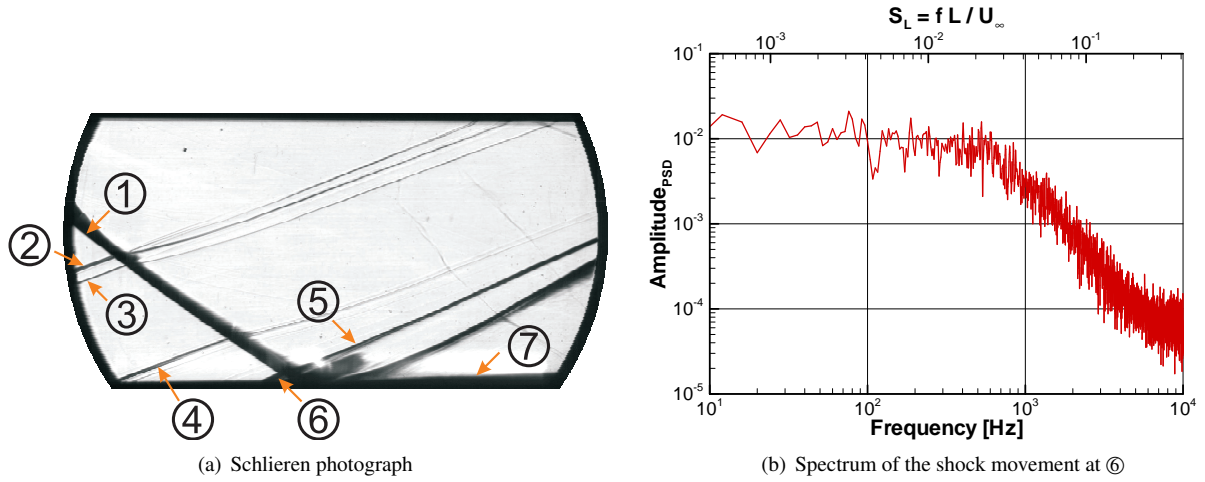
(a) Schlieren photograph

(b) Spectrum of the shock movement at ⑥

Figure 6: Schlieren photography of the shock wave boundary layer interaction at Mach 3.0

The experiments with a rigid panel allow a precise measuring of the pressure distribution of the shock wave boundary layer interaction. For several Mach numbers the measured values standardized with static pressure of the inflow (see tab. 2.2) are shown in figure 7(b). The elastic panel would range from $x = 0\,\text{mm}$ to $x = 300\,\text{mm}$. As expected the smaller the Mach number the earlier the shock hits the panel and the smaller is the relative pressure increase. But with respect to the static pressure values, the absolute pressure increase is bigger for smaller Mach numbers. The use of the ejector allows a reduction of the pressure level and therewith a reduction of the Reynolds number. But this does not change the shock position or the relative pressure increase. The PSI measurements at $y = 90\,\text{mm}$ reveal a shift of the interaction region and a lower pressure increase compared to the symmetry plane.

The oil film method facilitates a closer look on the flow topology in the region of the shock wave boundary layer interaction. On the left side of figure 5(b) the situation on the rigid panel is shown. The uniform parallel inflow, the curved shock, the separation region and some structures downstream are visible. In the symmetry plane the separation ranges from $x = 71.5\,\text{mm}$ to $x = 111.5\,\text{mm}$. These values agree with the measured pressure distributions.

(a) Numerical and experimental results at Mach 3.0

(b) Numerical and experimental results at several Mach numbers
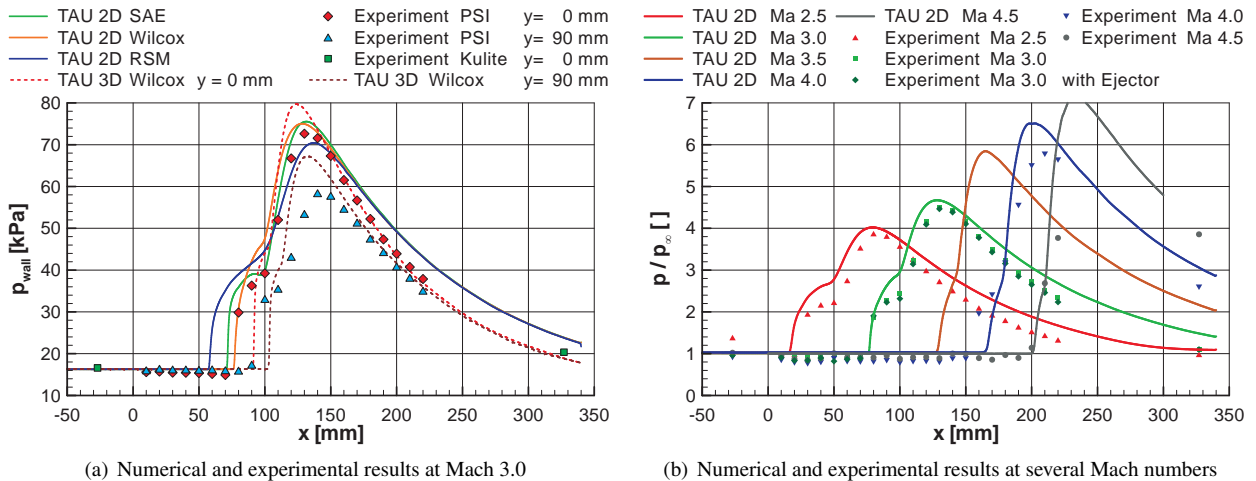
Figure 7: Pressure distribution of the shock wave boundary layer interaction on a rigid panel

5.2 Flow structure interaction

The structure deflection of the fluid structure interaction experiments divides into a large static deflection and small vibrations. The panel's load and therefore the static component of the panel deflection is directly connected to the pres-

(a) Static component for several pressure levels at Mach 3.0

(b) Spectrum at several pressure levels at Mach 3.0

(c) Static component for several wedge positions at Mach 3.0

(d) Spectrum at several wedge positions at Mach 3.0

(e) Static component for several Mach numbers

(f) Spectrum at several Mach numbers

Figure 8: Deflection of the elastic panel during the wind tunnel experiments

(a) Full spectrum of deflection and pressure

(b) Vibrational spectrum at two different sensor positions and without the wedge

Figure 9: Measured spectra at Mach 3.0 and the wedge at $y = 115\,\text{mm}$

sure level of the flow as shown in figure 8(a). A translational displacement of the wedge is attended by a translational displacement of the shock impingement and the pressure jump and therefore also a shift of the point of the maximum deflection. As a movement downstream reduces the summarized load it leads to a reduction of the static deflection (figure 8(c)). The increase of the Mach number leads to a decreasing pressure level (see tabular 2.2) as well as a shift of the shock impingement downstream (see figure 7(b)). Hence the maximum deflection decreases and its position moves downstream with an increasing Mach number as shown in figure 8(e). The figures 8(a), (c) and (b) also include calculations based on the modified second order beam equation as described in 4.1, the pressure distributions from 2D simulations shown in 7(b) and the measured back pressure during the experiments.
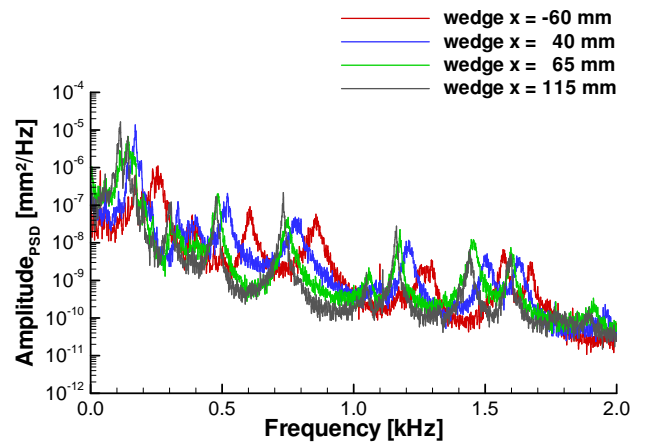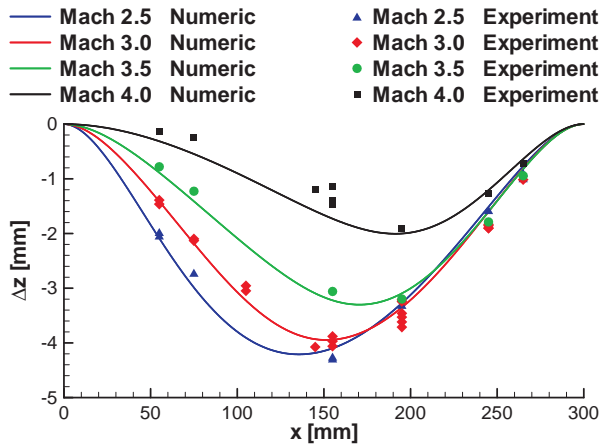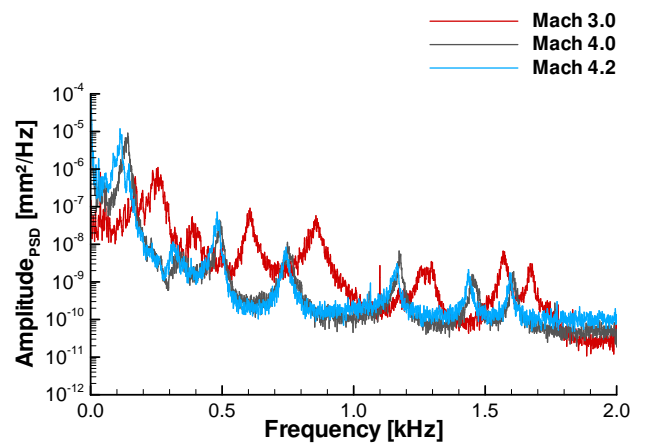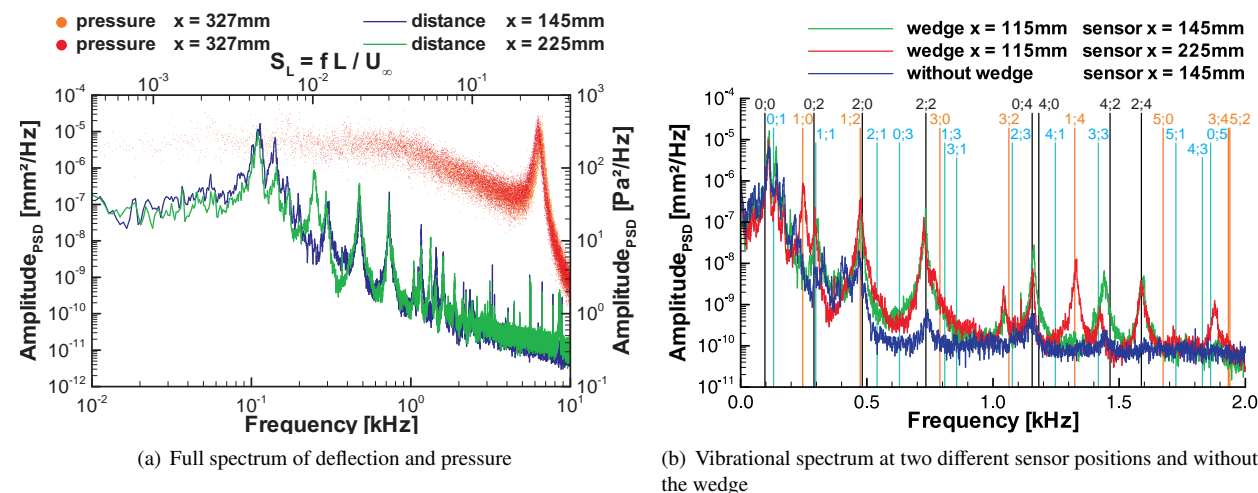
Figure 9(a) shows a full spectrum of the dynamic component of the structure deflection measured at two sensor positions. There are several peaks between $50\,\text{Hz}$ and $2\,\text{kHz}$ and thus in the range of the normal modes. In addition, there is a single peak at $8.5\,\text{kHz}$ for the sensor at position $225\,\text{mm}$.

A detailed look on the panel vibrations in the range of the normal modes gives figure 9(b) measured at Mach 3.0 and the wedge at $x = 115\,\text{mm}$. The movement of the wedge downstream leads to a smaller static panel deflection and therefore to larger vibration amplitudes. The plot shows the results of the capacitive sensor as it has a much lower noise level. Due to its size it can just be placed on the symmetry plane. In two identical runs it was placed once in the middle of the panel ($y = 145\,\text{mm}$) and once at three-fourths of the panel length ($y = 225\,\text{mm}$). The are several prominent peaks and most of them can be identified as a normal mode of the panel. Therefore the figure includes also the calculated frequencies for a uniform pressure load of $2000\,\text{Pa}$. The capacitive sensor cannot detect modes with an odd number in transversal direction (plotted in light blue) as they have a neutral line in the symmetry plane. In addition it neither can detect modes with an odd number in longitudinal direction (plotted in orange), if it is place in the middle of the panel, nor modes with a 3 or a 4 in longitudinal direction, if it is placed at $y = 225\,\text{mm}$, as they are also close to neutral lines. The good agreement of measured peaks and calculated values become especially apparent for the modes $1;0$ and $1;4$ as they are detected just at the non middle position. (This effect does not appear for the modes $1;1$ and $1;3$ as they have an odd number in transversal direction too or for mode $1;2$ as its frequency is very close to the frequency of mode $2;0$.) In comparison with Vedeneev et al. [20] much more and also higher modes could be surely identified. For a detailed discussion of the differences please see section 6.3.

The right side of figure 5(b) shows an oil flow picture on the elastic panel. The direct comparison to the rigid panel reveals that the shock on the elastic panel is much less bend. The separation ranges now from $x = 63\,\text{mm}$ to $x = 113\,\text{mm}$ and is about 25% longer. In addition coarser textures downstream the impingment zone are visible.

10

6. Discussion

6.1 Static and dynamic behaviour of the structure

The investigation of the structure deformation under a static uniform pressure load reveals that in spite of the simple design several effects have to be taken into account for a correct modelling. In contrast to a linear structure model the second order beam equation considering the geometric hardening gives a reasonable first approximation of the deflection in the symmetry plane. A 3D model including the deformation of the frame which carries the elastic panel clearly improves the prediction quality. But for the same deflection the measured tensile force in the panel is lower than predicted (fig.3(e)) and the measured deflection of the frame is greater than simulated (fig. 3(b)). This demonstrates that the frame is weaker than assumed and its consideration is mandatory for a correct simulation. In contrast to that the fixing by riveting can be neglected, since the influence of (ideal) rivets is apparently small.

The simulations as well as the experiments show that the deformation shape of the panel is nearly two-dimensional with just small variations in transversal direction. But the measured panel deflections as well as the measured tensile forces indicate an essential difference of the deformation shape in the transversal direction compared to the simulations. In the simulations the deformation at the free sides is bigger than in the middle whereas it is just the other way around in the experiments. This may be caused by the foam rubber sealing at the panel sides, which were not considered in the simulations.

6.2 Shock wave boundary layer interaction

The comparison of the measured and computed pressure distributions in figure 7(a) illustrate the sensitivity of this test case to the used turbulence model. Surprisingly the results of 2D simulations using the SAE or Wilcox-k-ω model are in better consistence with the measurements on the symmetry plane than the RSM model. In particular the RSM model predicts a larger flow separation which begins earlier. The 3D simulations used much coarser grids and probably therefore provides a smaller flow separation and a stronger pressure increase. But they catch the pressure decrease behind the shock impingement line much better as they consider the flow from the wind side to the lee side of the wedge around the side edges. As shown in figure 5(a) the delayed pressure increase away from the symmetry plane due to the bended shock is also captured correctly.

As shown in figure 6(b) the analysis of the high-speed Schlieren pictures did not reveal any prominent frequency as described by Dupont et al. [4]. Probably this is caused by too much low frequency noise as the amplitudes decrease for frequencies above 700 Hz, which correspond to the significant Strouhal number of 0.03 found by Dupont. The noise could be caused by vibrations in the Schlieren set-up and a low pixel resolution of the separation bubble. So this should be improved for future test campaigns. The spectra of the pressure sensors show an unexpected peak around 6.5 kHz, which corresponds to a Strouhal number of 0.27. This peak appears in all experiments with and without a shock impingement and independent from the panel deflection. Although the frequency varies no clear correlation could be found yet. Unfortunately it is above the cut-off frequency of the sensor and therefore an interpretation would be vague. It is interesting that there is also a similar high frequency peak in the panel deflection but at a frequency of 8.5 kHz. Unfortunately this is neither good for a detailed analysis nor consistent with the majority of experimental data, since it disappears when the sensor is placed in the middle of the panel.

6.3 Fluid structure interaction

The experimental data show that the flow deforms the structure and there is a reaction of the flow to the deflection hence there is a flow structure interaction.

The constant component of the panel deflection decreases with a decreasing pressure level, a downstream movement of the wedge and an increasing Mach number. The last two also cause a shift of the point of the maximum deflection downstream. Important is the total amount and the balance point of the pressure load. An increasing deformation increases also the tensile strains in the panel, which affects the normal modes and thereby the dynamic component of the structure deflection. But there are also some other effects as shown in 5.2. Most of the peaks in the spectrum of the panel deflection directly correspond to a normal mode but some break ranks (fig. 9(b)). The measured frequency of the mode 0; 0 is higher than simulated this can be explained with the high sensitivity of the this mode for the difference of the deformation shape in the simulation and the experiment due to the different pressure loads. It is striking that a significant frequency shift occurs just for the modes 3; 2, 4; 2 and 5; 2 always to lower frequencies. On the
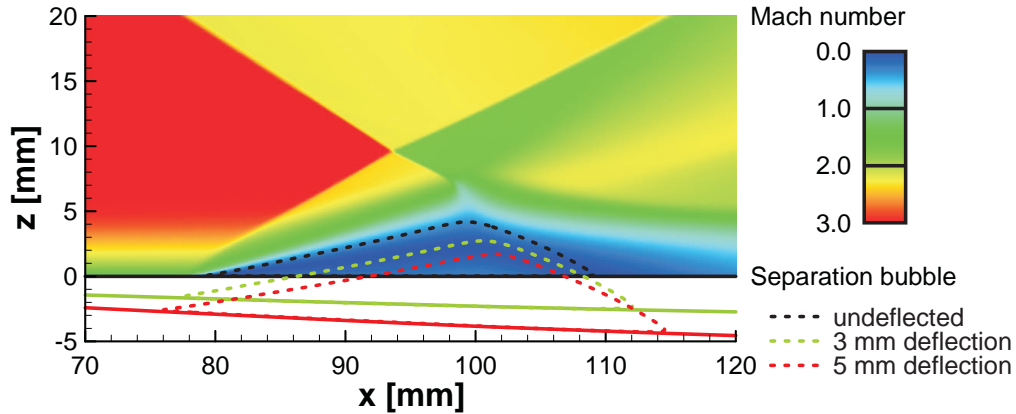
11

Figure 10: Computed separation bubble shapes for several defined deflections at Mach 3.0 and the Mach number distribution for the undeflected case

one hand all these modes have two neutral lines in transversal direction and therefore a connection to the deformation shape seems plausible but on the other hand the modes 0; 2, 1; 2 and 2; 2 are not effected.

The comparison of the two spectra in figure 9(b) with the sensor at the same position but one with the wedge at $y = 115\,\text{mm}$ and one without any wedge show that the frequencies are nearly the same but the amplitudes differ significantly. This is plausible as the deflection nearly same but the oscillating separation bubble causes a much higher excitation of the vibrations in the case with the wedge. This effect explains also the difference between figure 8(b) and figure 8(d). In both cases most of the flow characteristics as the size and the shape of the separation are unchanged but the deflection of the panel is reduced in figure 8(b) due to a reduction of the overall pressure level and in figure 8(d) due to a translational displacement of the wedge. Hence in both cases the frequencies of the normal modes decrease. In the case of the pressure reduction also the amplitudes decrease as the excitation through the separation bubble decreases with the pressure level whereas in the case of the wedge displacement the amplitudes increase as the excitation is constant but the tensile forces are reduced. As discussed before also an increase of the Mach number leads to a reduction of the panel deflection and again this leads to a reduction of the frequencies (fig. 8(f)) but this time the amplitude of some modes increase (1st and 5th) some decrease (2nd, 4th and 6th) and some are quite the same (3rd and 7th). This could be caused by a changing excitation due to a changed separation bubble.

The most evident reaction of the flow on the panel deflection is the straightening of the curved shock (fig. 5(b)). This is probably caused by arising corner vortices as the elastic panel does not span the whole wind tunnel width and a step forms between the elastic panel and the surrounding plate.

For the change of the separation bubble size the direct dependency to the deflection is proven by two-dimensional simulations as shown in figure 10. Although the size and the position are not predicted correctly, the enlargement matches quite well the measured values. The coarser textures of the oil flow picture on the elastic panel downstream the impingement zone indicate larger structures in the flow in particular stationary vortices probably also a consequence of the larger separation zone.

7. Summary

An experimental study concerning the fluid structure interaction has been carried out in the supersonic flow regime of the Trisonic Test Section (TMK) in Cologne. The focus of the investigations was a detailed characterization of the wind tunnel flow as well as a precise measurement of the shock wave boundary layer interaction and the structure deformation. The detailed analysis of the boundary conditions of the experiments provides a reliable basis for the validation of numerical simulations. The combination of a shock wave boundary layer interaction with a fluid structure interaction is challenging for modelling and therefore promises to be an adequate criterion.

To facilitate detailed and parametric numerical simulations one objective of the experimental set-up was a two-dimensional flow structure interaction. For several reasons this could not be achieved. The shock generator and the elastic panel of the test model do not span the whole wind tunnel width, which leads to a three-dimensional flow topology in the whole test volume. Because of its finite width and not ideally restrained grips the panel deformation is also three-dimensional. This leads to more complex measurements, analysis and simulations.

The measured data confirmed a flow induced structure deformation consisting of a big static component and small dynamic components with several dominant frequencies between 50 and 2000 Hz corresponding to the normal modes of the deflected panel. Although the amplitudes of the structure oscillation are very small, they showed direct dependencies to the excitation by the flow. For a better understanding of the mechanism and an explanation of some frequency shifts, further detailed analysis is necessary.

Although there is a measurable reaction of the flow to the deformation of the structure the dynamic aspects are not as evident as expected. Surprisingly no prominent frequencies in the Schlieren pictures were identified and the measured peak in the pressure spectrum is at unexpectedly high frequencies. For a better detection of any changes in the flow properties of future experiments, it is necessary to use faster pressure sensors and to improve the Schlieren photography.

To enhance the fluid structure interaction it is planned to build a new insert which hopefully generates vibrations with larger amplitudes. Therefore the frequency of one of the first panel's normal modes should coincides with a dominant frequency of the flow e.g. the separation oscillation.

Acknowledgements

References

[1] Bradski, G. and Kaehler, A. (2008). *OpenCV: Computer Vision with the OpenCV Library*. O'Reilly Media, Sebastopol, California, 1st edition.

[2] Danowski, C. and Wall, W. A. (2011). A monolithic approach to thermo-structure interaction in rocket nozzles. In *4th European Conference for Aerospace Science*, Saint Petersburg. EUCASS association.

[3] Dolling, D. S. (2001). Fifty Years of Shock-Wave/Boundary-Layer Interaction Research: What Next? *AIAA Journal*, 39(8):1517–1531.

[4] Dupont, P., Haddad, C., and Debiève, J. F. (2006). Space and time organization in a shock-induced separated boundary layer. *Journal of Fluid Mechanics*, 559:255–277.

[5] Esch, H. (1986). *Die 0,6-m X 0,6-m-Trisonische Meßstrecke (TMK) der DFVLR in Köln-Porz (Stand 1986)*. DFVLR-Mitteilungen. Deutsche Forschungs- und Versuchsanstalt für Luft- und Ramfahrt e.V., Köln.

[6] Estruch, D., Lawson, N. J., MacManus, D. G., Garry, K. P., and Stollery, J. L. (2008). Measurement of shock wave unsteadiness using a high-speed schlieren system and digital image processing. *The Review of scientific instruments*, 79(12):126108.

[7] Fluent (2006). *FLUENT 6.3 User's guide*. Fluent Inc., Lebanon, New Hampshire.

[8] Gerhold, T. (2002). Overview of the hybrid RANS code TAU. *Notes on Numerical Fluid Mechanics and Multidisciplinary Design*, 89:81–92.

[9] Grilli, M., Hickel, S., and Adams, N. A. (2011). Implicit Large Eddy Simulation of a Supersonic Turbulent Boundary Layer over a Compression-Expansion Ramp. In *4th European Conference for Aerospace Science*, Saint Petersburg. EUCASS association.

[10] Hagemann, G. (2009). Shock pattern in the plume of rocket nozzles: needs for design consideration. In Hannemann, K., editor, *26th International Symposium on Shock Waves*, volume 17, Göttingen.

[11] Humble, R. A., Elsinga, G. E., Scarano, F., and van Oudheusden, B. W. (2007). Investigation of the Instantaneous 3D Flow Organization of a Shock Wave/Turbulent Boundary Layer Interaction using Tomographic PIV. In *37th AIAA Fluid Dynamics Conference and Exhibit*, volume 4112 of *AIAA*, pages 1–16, Miami, Florida. American Institute of Aeronautics and Astronautics.

[12] Koschel, W. (2003). Flight 157- Ariane 5 ECA: Report of the Inquiry Board. Technical report, European Space Agency.

[13] Loving, D. L. and Katzoff, S. (1959). The Fluorescent-Oil Film Method and Other Techniques for Boundary-Layer Flow Visualization. Technical Report NASA MEMO 3-17-59L.

[14] Lüdeke, H., Calvo, J. B., and Filimon, A. (2006). Fluid Structure Interaction at the ARIANE-5 Nozzle section by Advanced Turbulence Models. In Wesseling, P., Onate, E., and Périaux, J., editors, *European Conference on Computational Fluid Dynamics*, pages 1–16, Delft. TU Delft.

[15] Reijasse, P. and Poutrel, R. (2005). Flow Separation Regimes Induced by Cap-Shock in Over-Expanded Optimized Propulsive Nozzles. In *1st European Conference for Aerospace Sciences (EUCASS)*, pages 10–13, Moscow. EUCASS.

[16] Ruf, J. H., Brown, A. M., and McDaniels, D. M. (2004). Nozzle Side Load Testing and Analysis at Marshall Space Flight Center. In *45th AIAA/ASME/SAE/ASEE Joint Propulsion Conference*, Denver, Colorado. American Institute of Aeronautics and Astronautics.

[17] Schieffer, G., Hosters, N., Klaus, M., Behr, M., and Reimerdes, H.-G. (2011). Towards Aerothermoelastic Simulations of Supersonic Flow through Nozzles. In *4th European Conference for Aerospace Sciences*, Saint Petersburg. EUCASS association.

[18] Schodl, R. (1979). Development of the laser two-focus method for non-intrusive measurement of flow vectors particularly in turbomachines. PhD thesis ESA-TT-528, European Space Agency, Paris (France).

[19] Storti, M. a., Nigro, N. M., Paz, R. R., and Dalcín, L. D. (2009). Strong coupling strategy for fluid-structure interaction problems in supersonic regime via fixed point iteration. *Journal of Sound and Vibration*, 320(4-5):859–877.

[20] Vedeneev, V. V., Guvernyuk, S. V., Zubkov, A. F., and Kolotnikov, M. E. (2010). Experimental observation of single mode panel flutter in supersonic gas flow. *Journal of Fluids and Structures*, 26(5):764–779.